Electronic Supplementary Information

Highly Efficient Broadband Photodetectors Based on the Lithography-Free $Au/Bi_2O_2Se/Au$ Heterostructures

Xiaolong Liu,[a] Ruiping Li,[b] Chengyun Hong,[a] Gangfeng Huang,[a] Danfeng Pan,[c,*] Zhenhua Ni,[d] Yongqing Huang,[e] Xiaomin Ren[e], Yingchun Cheng[b,*] & Wei Huang[b,f]

a. State Key Laboratory of Alternate Electrical Power System with Renewable Energy Sources and Beijing Key Laboratory of Energy Safety and Clean Utilization, Renewable Energy School, North China Electric Power University, Beijing 102206, China.

b. Key Laboratory of Flexible Electronics & Institute of Advanced Materials, Jiangsu National Synergetic Innovation Center for Advanced Materials, Nanjing Tech University, 30 South Puzhu Road, Nanjing 211816, China.

c. National Laboratory of Solid State Microstructures, School of Electronic Science and Engineering Collaborative Innovation Center of Advanced Microstructures, Nanjing University, Nanjing 210093, China.

d. Department of Physics, Southeast University, Nanjing 211189, China

e. State Key Laboratory of Information Photonics and Optical Communications, Beijing University of Posts and Telecommunications, Beijing 100876, China

f. Shaanxi Institute of Flexible Electronics (SIFE), Northwestern Polytechnical University, 127 West Youyi Road, Xi'an, 710072, China

The Corresponding authors:

*E-mail: iamyccheng@njtech.edu.cn

*E-mail: pdf@nju.edu.cn

Supporting Information

1. The crystal structure of the Bi_2O_2Se films, the device optical and AFM characterizations under different annealing temperatures
2. The device performance before annealing
3. The details of the Bi_2O_2Se energy band structure calculation
4. The details of the device for photocurrent mapping in Fig. 1 and Fig. 2
5. The output curves of the device in Fig. 3 in the linear and logarithm coordinates under the dark and laser illumination conditions
6. The enlarged spectral photocurrent curve of Fig. 3c, the enlarged photocurrent curve of Fig. 3d under laser on/off modulation to amplify the I_{ph} rising edge
7. The optical and AFM images of the device with 0.8 μm channel length in Fig. 4, the I_{ph} mapping with intense scale bar
8. The device performance with 200℃ annealing
9. The comparison between the performances of the Bi_2O_2Se photodetectors.

1. The crystal structure of the Bi_2O_2Se films, the device optical and AFM characterizations under different annealing temperatures

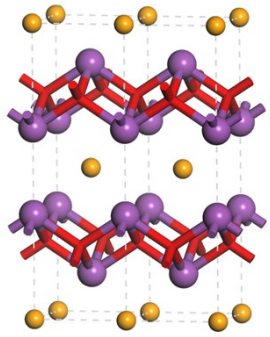

Figure. S1 The schematic illustration of the Bi_2O_2Se crystal structure.

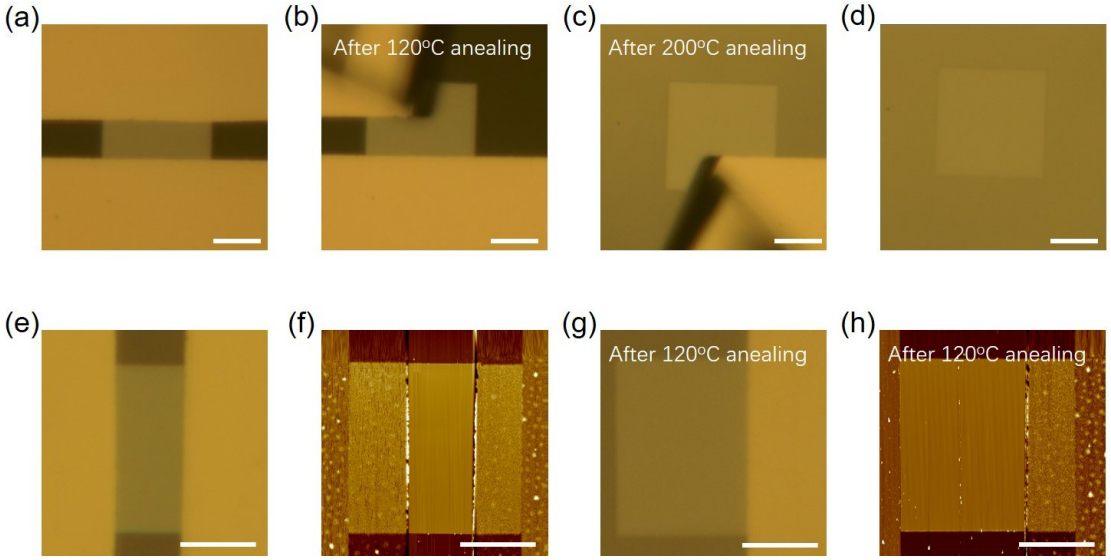

Figure. S2 The device optical microscopic and AFM characterizations, the upper and lower columns correspond to two different devices. (a) The optical microscope image of the device before annealing. (b) After 120℃ annealing, the electrode could be peeled up with a probe tip. (c) With the elevated annealing temperature of 200℃, the other electrode could still be removed with the probe tip. (d) The remaining square Bi_2O_2Se film is contaminant-free from the optical image. (e) The optical image of another Au/Bi_2O_2Se/Au device adopting the same electrode fabrication method. (f) The AFM characterization of the device in Fig. S2e. (g) The optical microscope image of the device in Fig. S2e after 120℃ annealing and with one electrode peeled away. (h) The AFM

characterization corresponds to the optical image in Fig. S2g. The scale bar is 10μm.

2. The device performance before annealing

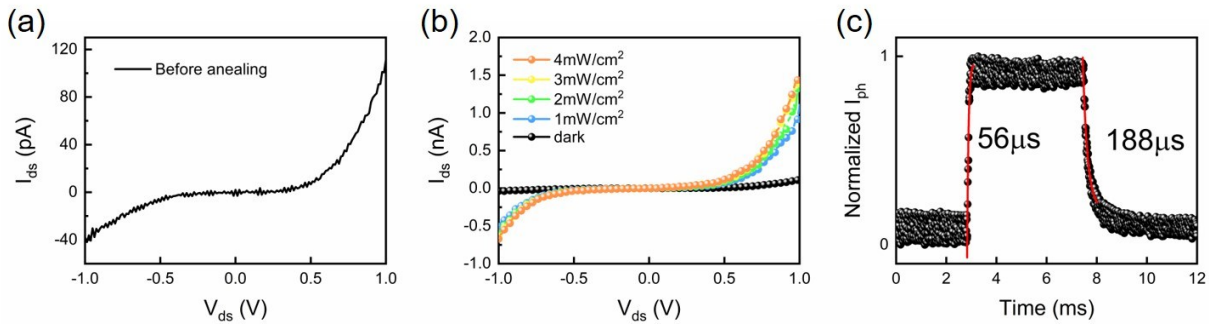

Figure. S3 (a) The output curve of the device before annealing under dark condition. (b) The I-V curves under 640nm laser with different power densities. (3) The device dynamic response. With single exponential fitting, the lifetime at the rising and decay edges are 56μs and 188μs separately.

3. The details of the Bi_2O_2Se energy band structure calculation and the transfer curve of the Bi_2O_2Se FETs on SiO_2/Si substrates.

The calculation of the Bi_2O_2Se energy band structure was based on the density functional theory with the QUANTUM-ESPRESSO package [1]. Generalized gradient approximation (GGA) with Perdew-Burke-Ernzerhof (PBE) exchange and correlation functional parameterization [2] was used. The location of the conduction band edge (E_c), the valence band edge (E_v) and the work function were calculated with ultra-soft pseudopotentials [3] utilized for elements Bi, O and Se. Kinetic energy cutoff of 544 eV, the Monkhorst-Pack *k*-mesh of $4 \times 4 \times 1$, and convergence threshold on energy of 2.72×10^{-3} eV were used. The calculations were carried out on the 6L Bi_2O_2Se film considering that the band gap of 6L Bi_2O_2Se is close to the bulk phase [4]. The obtained E_c is -4.73 eV, E_v is -5.35 eV, while the work function of Bi_2O_2Se is 4.73~5.04 eV considering that Bi_2O_2Se is overwhelmingly n-doped. The work function Au of 5.1eV was also calculated from the QUANTUM-ESPRESSO code [5]. Then the energy band alignment of Au and Bi_2O_2Se could be depicted as in Figure. 1f and 1g.

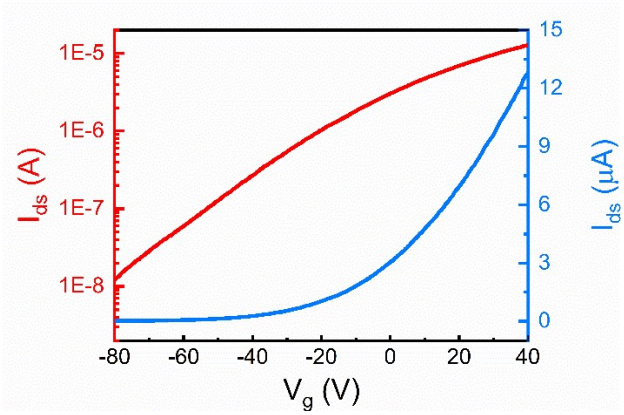

Figure. S4 The Bi_2O_2Se film grown on the *f*-mica flakes was transferred on the SiO_2/Si substrates and the FETs was fabricated with Au as the electrodes. The transfer curve was depicted here in both the linear and logarithmic scale, colored in blue and red respectively.

4. The details of the device for photocurrent mapping in Fig. 1 and Fig. 2

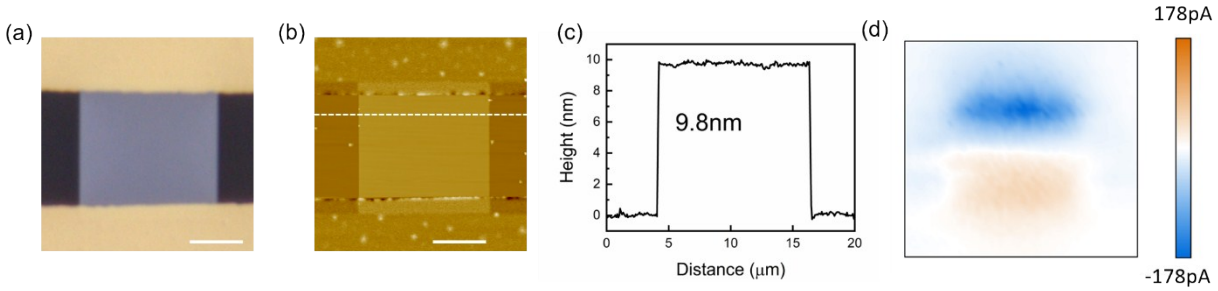

Figure. S5 (a) The optical microscope image of the device with 120℃ annealing adopted for photocurrent mapping in Fig. 1 and Fig. 2. (b) The AFM characterization result. (c) The Bi_2O_2Se thickness was 9.8nm measured along the white dash line in (b). The scale bar in (a) and (b) is 5μm. (d) The I_{ph} mapping image with the intense scale bar as in Fig. 1e.

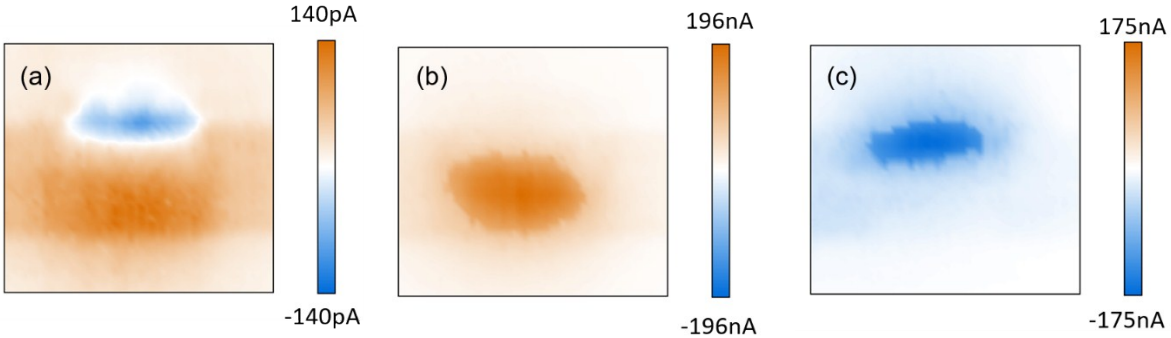

Figure. S6 The I_{ph} mapping images with the intense scale bar as the results in Fig. 2.

5. The output curves of the device in Fig. 3 in the linear and logarithm coordinates under the dark and laser illumination conditions

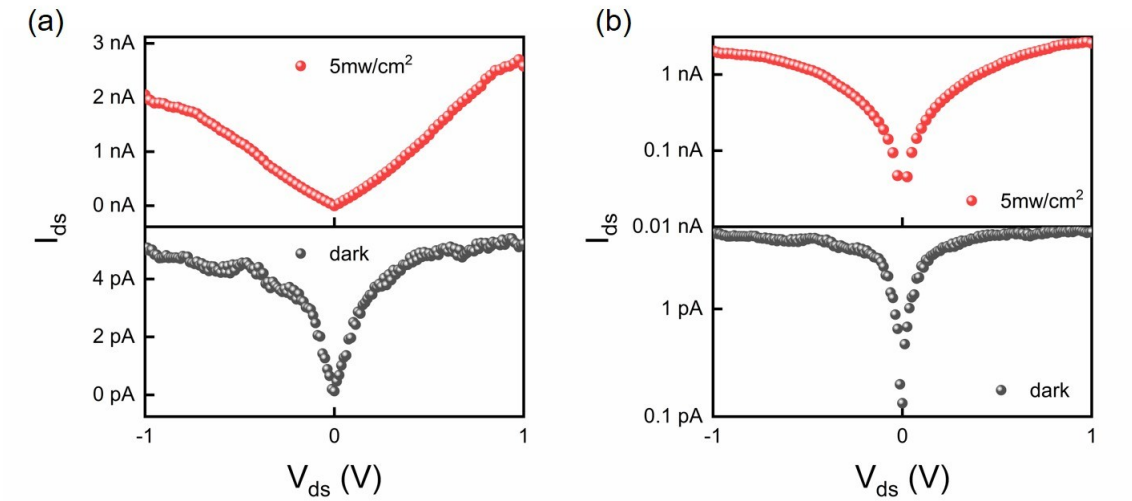

Figure. S7 (a) The linear I-V curves under dark (lower panel) and 5mW/cm^2 640nm laser illumination (upper panel). (b) The I-V curves in logarithm coordinate under dark (lower panel) and 5mW/cm^2 640nm laser illumination (upper panel).

6. The spectral photocurrent curve corresponds to the R~λ result in Fig. 3c, the enlarged photocurrent curve of Fig. 3d under laser on/off modulation to amplify the I_{ph} rising edge

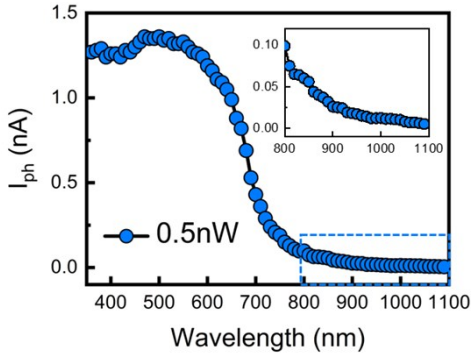

Figure. S8 The spectral I_{ph}~λ results correspond to Fig. 3c. The region from 800nm to 1090nm

was enlarged as the inset.

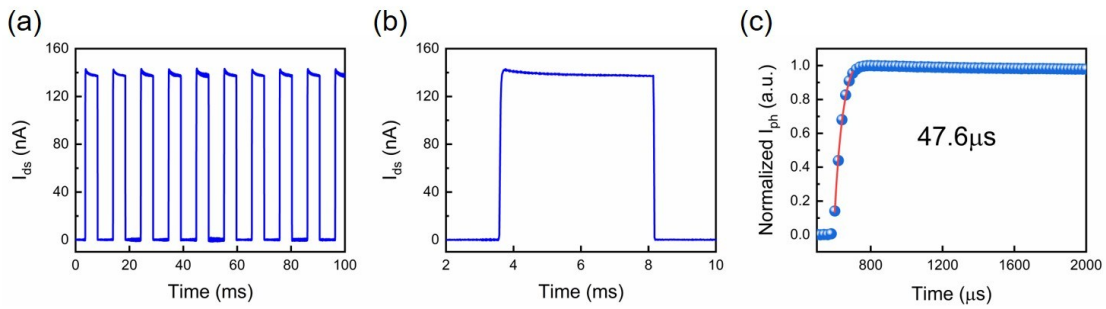

Figure S9 (a) Photocurrent under 640nm laser on/off modulation. (b) The enlarged first photocurrent "square wave" in (a). (c) exponential fitting of the I_{ph} rising edge in (b) with the response time of 47.6μs.

7. The optical and AFM images of the device with 0.8 μm channel length in Fig. 4, the I_{ph} mapping with intense scale bar.

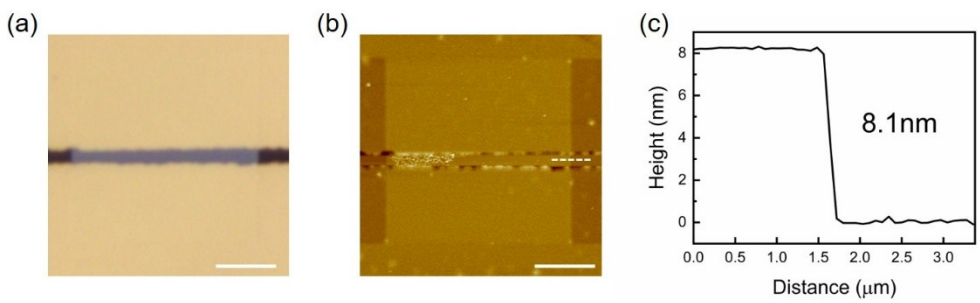

Figure. S10 (a) The optical microscope image of the device with 0.8μm channel length annealed by 120℃. (b) The corresponding AFM characterization result. (c) The Bi_2O_2Se thickness was 8.1nm measured along the white dash line in (b). The scale bar in (a) and (b) is 5μm.

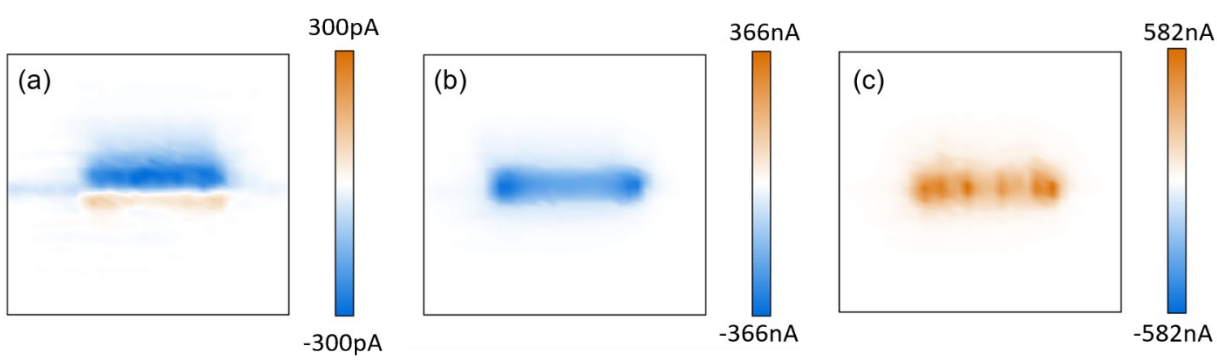

Figure. S11 The I_{ph} mapping results with the intense scale bar as in Fig. 4.

8. The device performance with 200℃ annealing

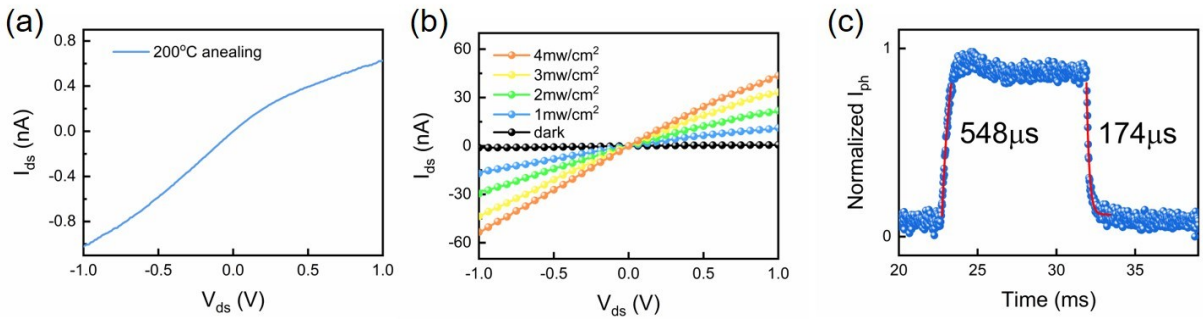

Figure. S12 (a) The output curve of the device annealed at 200℃. (b) The I-V curves under 640nm laser with different power densities. (3) The device dynamic response. With single exponential fitting, the lifetime at the rising and decay edges are 548μs and 174μs respectively.

9. The comparison between the performances of the Bi_2O_2Se photodetectors.

Device structure	Device response time (us)	Responsivity (A/W)	Wavelength (nm)	Detectivity (Jones)	Ref.
Evaporated Cr (SiO_2 substrate)	448	70000	532	3.0×10^{13}	S6
Evaporated Cr (SiO_2 substrate)	20000	22100	660	3.4×10^{15}	S7
Evaporated Ti (SiO_2 substrate)	/	65	1200	3.0×10^{9}	S8
Evaporated Cr (mica substrate)	2800	6.5	808	8.3×10^{11}	S9
Transferred Au (mica substrate)	36	9.1	640	1.3×10^{8}	This work

Table. S1 The comparison of the performances of the Bi_2O_2Se photodetectors, among these works, devices on the SiO_2/Si substrates exhibited larger responsivity with the electrical gating effects, though on the mica substrates, Bi_2O_2Se photodetectors were much faster.

References:

[1] Giannozzi, P.; Baroni, Stefano.; Bonini, N.; *et al.* QUANTUM ESPRESSO: a modular and

open-source software project for quantum simulations of materials. *J. Phys: Condens. Mat.* **2009**, *21*, 395502.

[2] Perdew, J. P. et al. Generalized gradient approximation made simple. *Phys. Rev. Lett.* **1996**, *77*, 3865.

[3] Vanderbilt, D. Soft self-consistent pseudopotentials in a generalized eigenvalue formalism. Phys. Rev. B **1990**, *41*, 7892.

[4] Wu, J.; Tan, C.; Tan, Z.; Liu, Y.; Yin, J.; Dang, W.; Wang, M.; Peng, H. Controlled Synthesis of High-Mobility Atomically Thin Bismuth Oxyselenide Crystals. *Nano Lett.* **2017**, *17*, 3021-3026.

[5] Wang, X.; Zebarjadi, M.; Esfarjani, K. First principles calculations of solid-state thermionic transport in layered van der Waals heterostructures. *Nanoscale* **2016**, *8*, 14695.

[6] Q. Fu, C. Zhu, X. Zhao, X. Wang, A. Chaturvedi, C. Zhu, X. Wang, Q. Zeng, J. Zhou, F. Liu, B. K. Tay, H. Zhang, S. J. Pennycook and Z. Liu, *Adv. Mater.* **2019**, *31*, e1804945.

[7] U. Khan, Y. Luo, L. Tang, C. Teng, J. Liu, B. Liu and H. -M. Cheng, *Adv. Funct. Mater.* **2019**, *29*, 1807979.

[8] J. Yin, Z. Tan, H. Hong, J. Wu, H. Yuan, Y. Liu, C. Chen, C. Tan, F. Yao, T. Li, Y. Chen, Z. Liu, K. Liu and H. Peng, *Nat. Commun.*, **2018**, *9*, 3311.

[9] J. Li, Z. Wang, Y. Wen, J. Chu, L. Yin, R. Cheng, L. Lei, P. He, C. Jiang, L. Feng and J. He, *Adv. Funct. Mater.*, **2018**, *28*, 1706437.